UPTEC F07 007
Examensarbete 20 p
16:e Januari 2007

Statistics Of The Energy Transfer From The Solar Wind To The Magnetosphere

Johan Falkenström

UPPSALA
UNIVERSITET

Teknisk- naturvetenskaplig fakultet
UTH-enheten

Besöksadress:
Ångströmlaboratoriet
Lägerhyddsvägen 1
Hus 4, Plan 0

Postadress:
Box 536
751 21 Uppsala

Telefon:
018 – 471 30 03

Telefax:
018 – 471 30 00

Hemsida:
http://www.teknat.uu.se/student

Abstract

Statistics Of the Energy Transfer From the Solar Wind To the Magnetosphere

Johan Falkenström

Our planet is strongly influenced by the Sun. Intense and time varying magnetic fields embedded in the outflowing solar wind can couple with the terrestrial magnetic fields leading to energy transfer between the solar wind and our magnetosphere. One of the main tasks in space physics research is to increase the knowledge of the spatial and temporal variation of this coupling and its influence on solar wind parameters and the interplanetary magnetic field.

Previously the energy input to the magnetosphere has been estimated with various coupling functions derived from solar wind measurements. However, with the multi-spacecraft mission Cluster there are improved techniques to determine the local energy transfer directly by in-situ measurements.

We use the multi-spacecraft mission Cluster to make observational estimates of the local energy transfer across the magnetopause. 15 magnetopause crossings at different spatial locations and during varying interplanetary conditions have been investigated. We attempt to determine the spatial dependence of the local energy transfer and the influence of varying interplanetary magnetic field conditions on the estimated energy transfer magnitude.

The local energy transfer is found to be positive, i.e. transferred from the magnetic field to the particles, as expected when Cluster is close to a reconnection region and detects high-speed plasma jets. When Cluster is located on the flanks of the magnetopause the energy input is strongly dependent on the location and on interplanetary conditions. For southward IMF the energy transfer is negative corresponding to the inflow of energy from the solar wind to the magnetosphere and varies with the magnitude of the southward component and the spatial location of the observation. For northward IMF there is positive energy flow close to reconnection zones otherwise no or little energy flow across the magnetopause flanks.

The observations are in good agreement with the current understanding on where and how the energy is transferred across the magnetopause. However, a larger statistical set of magnetopause crossings is needed in order to draw quantitative conclusions on the interplanetary as well as spatial dependence on the magnitude of the local energy transfer.

Handledare: Lisa Rosenqvist
Ämnesgranskare: Andris Vaivads
Examinator: Tomas Nyberg
ISSN: 1401-5757, UPTEC F07 007

Contents

Chapter 1

Introduction

Our planet is strongly influenced by the Sun. Intense and time varying magnetic fields embedded in the outflowing solar wind can couple with the terrestrial magnetic field leading to energy transfer between the solar wind and our magnetosphere. The variability of this energy coupling is reflected in rapid variations in the direction and intensity of the Earth magnetic field in the form of geomagnetic storms and substorms. One of the main tasks in space physics research is to increase the knowledge of the spatial and temporal variation of this coupling and understand the dependence of the solar wind parameters and the interplanetary magnetic field.

Previously the energy input to the magnetosphere has been estimated with various coupling functions derived from solar wind measurements, see e.g. [1]. However, with the multi-spacecraft mission Cluster there are improved techniques to determine the local energy transfer directly by in-situ measurements at the magnetopause.

The aim of this diploma work is to utilise the large data base of Cluster data to investigate the dependence of the local energy input from the solar wind on the spatial location at the magnetopause and validate an existing energy flux theory[4]. Furthermore, we investigate the dependence of local energy input on the variation of solar wind and interplanetary parameters such as the solar wind velocity, density, interplanetary magnetic field orientation and so on.

The outline is as follows, in the next chapter we discuss the space environment starting with an introduction to plasma physics. This lays as a foundation to explain concepts like the *interplanetary magnetic field* and the *solar wind*. In the third chapter we move closer to the Earth and discuss about the *magnetosphere* and how energy can be transfered between the solar wind and magnetosphere. The instrumentation and techniques used is presented in chapter 4. In chapter 5 the results of the current study are presented and discussed.

Chapter 2

Space-environment

Most matter in the universe is in a plasma state, from the interior of a star to a gaseous nebulae to the soft glow of the Aurora Borealis and the light from a fluorescent tube. Therefore a large part of this chapter will be devoted to a discussion around plasmas, where some important ideas and theorems will be deduced. This will then be used to introduce phenomena like the *solar wind* and *Interplanetary Magnetic Field* (IMF).

2.1 Plasmas

A plasma is defined as a *quasineutral gas of charged and neutral particles which exhibits collective behaviour*. Quasineutrality means that any externally introduced charge electric potential will be shielded out by the particles in the plasma, thus keeping the plasma as a whole in a neutral state. This shielding is called *Debye shielding*, and the thickness of this shielding is called the *Debye length*, defined as $\lambda_d = \left(\frac{\epsilon_0 K T_e}{ne^2}\right)^{1/2}$. Here KT_e is the thermal energy of the electrons in the plasma and n is the density of the plasma far away from the potential. In figure 2.1 the concept of Debye shielding is illustrated along with the Debye length. The collective behaviour of a plasma occurs since the particles in the plasma are electrically charged and when the particles move they generate electromagnetic fields $(\mathbf{B}, \mathbf{E})$. These fields then affect other particles in the plasma which starts to move and generate their own electromagnetic fields, and so on. Thus a small perturbation of a plasma might cause changes at great distances from the perturbed area due to these internal electric fields.

Since the plasma is electrically charged the governing equations will be Maxwell's equations

$$\nabla \times \mathbf{B} = \mu_0 \mathbf{j} + \epsilon_\mathbf{0}\mu_\mathbf{0}\frac{\partial \mathbf{E}}{\partial \mathbf{t}}, \tag{2.1}$$

$$\nabla \times \mathbf{E} = -\frac{\partial \mathbf{B}}{\partial t}, \tag{2.2}$$

$$\nabla \cdot \mathbf{B} = 0, \tag{2.3}$$

$$\nabla \cdot \mathbf{E} = \frac{\rho}{\epsilon_0}, \tag{2.4}$$

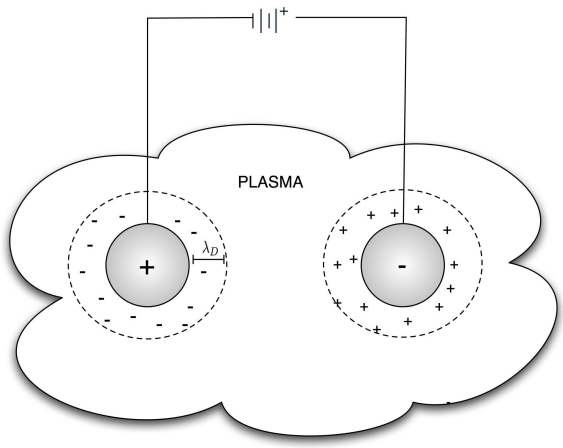

Figure 2.1: Debye shielding and the Debye length λ_D.

where $\mathbf{j}$ is the electric current density in a plasma, ρ the density and ϵ_0 and μ_0 are the vacuum permittivity and susceptibility respectively. Using Ohms law

$$\mathbf{j} = \sigma_0(\mathbf{E} + \mathbf{v} \times \mathbf{B}) \Rightarrow \mathbf{E} + \mathbf{v} \times \mathbf{B} = \eta \mathbf{j}, \tag{2.5}$$

where η is the plasma resistivity, we can make a very important definition regarding plasmas. When a plasma is highly conducting, i.e. when $\sigma_0 \to \infty \Leftrightarrow \eta \to 0$, we can approximate this to

$$\mathbf{E} + \mathbf{v} \times \mathbf{B} = 0. \tag{2.6}$$

This is called the *ideal Magneto-Hydro-Dynamic* (ideal MHD) approximation. In this approximation the different interactions between the particles in the plasma are neglected, what is gained are equations that are possible to solve analytically. Returning to Ohm's law, but this time using equation 2.2 to rewrite it as

$$\frac{\partial \mathbf{B}}{\partial t} = \nabla \times (\mathbf{v} \times \mathbf{B} - \frac{\mathbf{j}}{\sigma_\mathbf{0}}). \tag{2.7}$$

Assuming that the plasma velocity is much smaller than the speed of light, meaning that we can neglect displacement currents, equation 2.1 can be rewritten as

$$\mathbf{j} = \frac{\mathbf{1}}{\mu_\mathbf{0}} \nabla \times \mathbf{B}.$$

Using this equation with equation 2.7 we get

$$\frac{\partial \mathbf{B}}{\partial t} = \nabla \times (\mathbf{v} \times \mathbf{B}) - \frac{\mathbf{1}}{\mu_\mathbf{0}\sigma_\mathbf{0}} \nabla \times (\nabla \times \mathbf{B}),$$

now using equation 2.3 and some basic differential relations we get the result

$$\frac{\partial \mathbf{B}}{\partial t} = \nabla \times (\mathbf{v} \times \mathbf{B}) + \frac{\mathbf{1}}{\mu_\mathbf{0}\sigma_\mathbf{0}} \nabla^\mathbf{2} \mathbf{B}. \tag{2.8}$$

This equation can further be reduced assuming an ideal MHD plasma to

$$\frac{\partial \mathbf{B}}{\partial t} = \nabla \times (\mathbf{v} \times \mathbf{B}). \tag{2.9}$$

This equation highlights a very important feature in the MHD approximation, the magnetic field lines are *frozen-in* to the plasma. The validity of the MHD approximation can be expressed by the so called magnetic Reynolds number

$$R_m \equiv \mu_0 \sigma_0 L_B V \tag{2.10}$$

where V is the plasma flow speed and L_B the characteristic length over which the field varies. A high Reynolds number indicates large scales and high conductivity, the basis of a valid MHD approximation. A Reynolds number comparable to unity indicates that the MHD approximation is not valid.

2.2 The solar wind and the interplanetary magnetic field

The solar wind is a continuous but fluctuating stream of plasma ejected from the Sun mainly constituting of hot electrons and protons. Since the length scales in space physics are enormous and the plasma ejected has a high conductivity, the solar magnetic field will get dragged by the solar wind, due to the frozen-in concept, creating the IMF. To realise the validity of using the frozen-in concept in the context of the solar wind lets examine the total distance the magnetic fields are able to diffuse in a typical solar wind plasma. The density is of the order $5cm^{-3}$ with a temperature of about 50 eV, which yields a diffusion time of $\tau_d \approx 0.3L_B^2$, using the Spitzer resistivity, $\eta \approx \frac{\pi e^2 m^{1/2}}{(4\pi\epsilon_0)^2 (KT_e)^{3/2}} ln(12\pi n \lambda_D^3)$. Here m is the total electron mass. The typical velocity of the solar wind is 500 km/s, which means that the time needed to propagate to Earth, $1.5 \cdot 10^{11}$ m away, is 3.5 days. Using this value as the magnetic diffusion time one find that the magnetic fields in the solar wind are permitted to diffuse only 10^3 m. Hence, the magnetic fields are practically frozen in to the solar wind. Thus, using the MHD approximation when performing calculations of solar wind plasma is perfectly valid. Since the Sun rotates every 27 days it drags the IMF along effectively twisting it in a Archimedean pattern called the Parker spiral, figure 2.2.

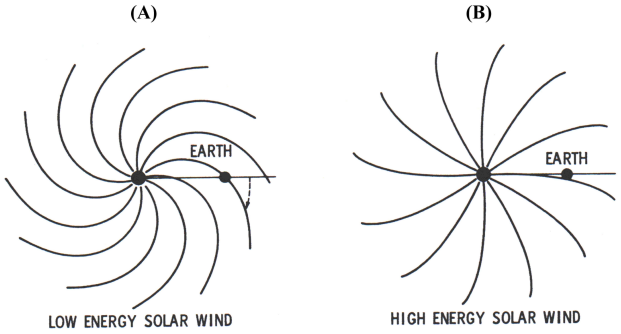

Figure 2.2: The Parker spiral during (A) a low energy solar wind and (B) a high energy solar wind

Chapter 3

Near-Earth environment

The near Earth environment is defined as the area inside the magnetosphere and in the vicinity of the magnetopause. Since all the physics regarding the coupling between the IMF and the terrestrial magnetic field happens in this region this chapter is fairly long and descriptive. It starts with a description of some of the different regions in the magnetosphere and the system of currents that is contained therein. Furthermore it explains the basic idea of the very complex concept of magnetic reconnection. Last there is a theoretical deduction of the energy conversion expression that is the foundation of this report.

3.1 The Magnetosphere

Earth's magnetic field is approximately a magnetic dipole with the north pole tilted by about 11° from the rotational axis. It is believed that the field is sustained by the so called dynamo theory, where Coriolis forces affect molten iron and nickel in the outer planetary core together with convection. When these highly conductive fluids flow over an existing magnetic field a current is induced which helps to reinforce the original magnetic field. It is possible to define a coordinate system using the magnetic properties of the Earth. This system is called the *Geocentric Solar Magnetic* (GSM) system, $(\hat{\mathbf{x}}_{gsm}, \hat{\mathbf{y}}_{gsm}, \hat{\mathbf{z}}_{gsm})$. Here $\hat{\mathbf{x}}_{gsm}$ is directed towards the sun, $\hat{\mathbf{z}}_{gsm}$ directed along the magnetic north pole. Ofcoarse the $\hat{\mathbf{y}}_{gsm}$ axis will be directed perpendicular to both $\hat{\mathbf{x}}_{gsm}$ and $\hat{\mathbf{z}}_{gsm}$ in the Dawn-to-Dusk direction.

When the super-sonic solar wind hits this magnetic field, a bow shock is created where the plasma is slowed down and thermalized. The plasma in the region behind the bow shock is deflected around Earth's magnetic field due to the frozen in condition, forming what is known as the magnetosheath, see figure 3.1. The kinetic pressure from plasma in the magnetosheath compress the Earth's magnetic field on the day side and stretch the field on the night side, this bullet shaped cavity is called the magnetosphere. The boundary separating the magnetosheath from the magnetosphere is called the magnetopause, this is where the thermal, magnetic and dynamic pressure in the magnetosheath and in the magnetosphere are at an equilibrium state. Since the solar wind is strongly fluctuating the pressure in the magnetosheath is constantly changing thus the location of the magnetopause is shifting. This boundary plays an important

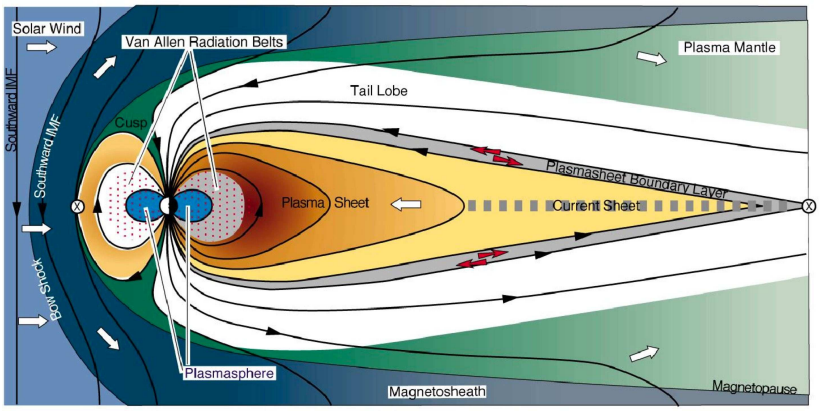

Figure 3.1: The magnetosphere and the different regions within it

role in solar-terrestrial physics since it is the surface through which the coupling between the solar wind and the magnetosphere occurs. Closer to Earth we have the plasmasphere populated by a high density plasma that co-rotates with the Earth. Encapsulating the plasma sphere is the Van Allen radiation belts which constitutes mostly of high energy electrons [8] which moves along the dipolar field lines.

The electric and magnetic fields in the magnetosphere will cause particles to drift perpendicular to the magnetic field lines according to the following expression:

$$\mathbf{V}_D = \left(\frac{\mathbf{E}\times\mathbf{B}}{B^2}\right) + \frac{w_\perp}{qB^2}\left(\mathbf{B}\times\nabla B\right) + \frac{2w_\parallel}{qR_c^2B^2}\left(\mathbf{R}_c\times\mathbf{B}\right) \tag{3.1}$$

where $w_\perp$ and $w_\parallel$ are the particles perpendicular and parallel energies, respectively, and $\mathbf{R}_c$ is the local radius of the magnetic field lines. The first of the equations on the right hand side is the $E\times B$ drift, named after the fact that the drift is perpendicular to both the electric and magnetic fields. The second term is called the *gradient drift* due to the fact that the particles drifts in the direction perpendicular to both the magnetic field and the gradient of the magnetic field. The last part of the equation is the so called *curvature drift* since in contributes to a component in a direction perpendicular to both the curvature of the magnetic field and the magnetic field itself. As the gradient drift and curvature drift flow perpendicular to both the curvature of the magnetic field and to the magnetic field itself and both depend on the particles charge, ions and electrons will flow in different directions and currents will develop. These currents is part of a complex system of currents flowing in the magnetosphere, see 3.2.

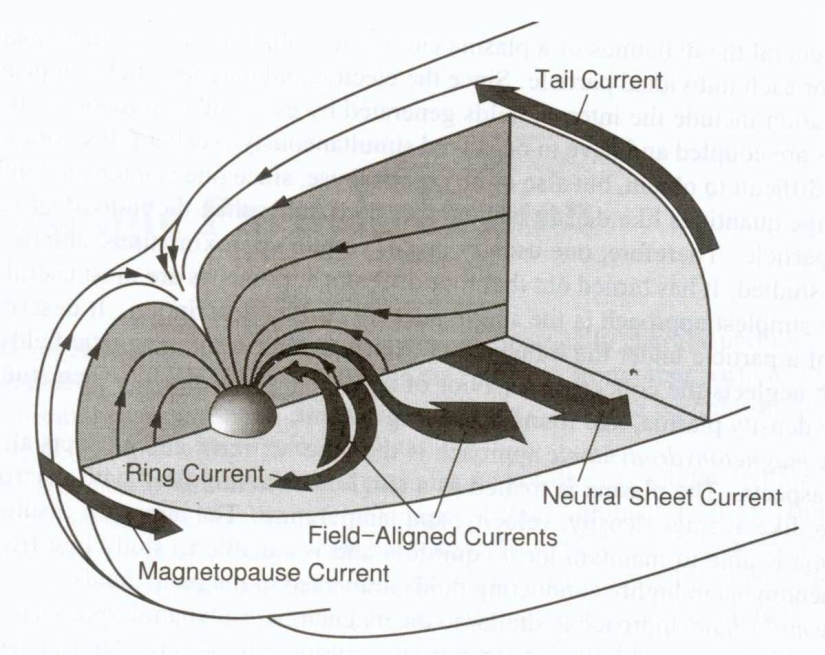

Figure 3.2: Some of the currents and their direction in the magnetosphere

Another important current occurs at the magnetopause, where the transition between the highly compressed, weakly magnetized, solar wind plasma to the low density, highly magnetized, magnetospheric plasma causes a current to flow across the magnetopause. This can be realized by using Ampere's law

$$\frac{1}{\mu_0}\nabla \times \mathbf{B} = \mathbf{j}$$

expanding the cross product we get

$$\frac{1}{\mu_0}\nabla \times \mathbf{B} = \frac{1}{\mu_0}\begin{vmatrix} \hat{x} & \hat{y} & \hat{z} \\ \frac{\partial}{\partial x} & \frac{\partial}{\partial y} & \frac{\partial}{\partial z} \\ B_x & B_y & B_z \end{vmatrix} =$$
$$\frac{1}{\mu_0}\left[\left(\frac{\partial B_z}{\partial y} - \frac{\partial B_y}{\partial z}\right)\hat{x} - \left(\frac{\partial B_z}{\partial x} - \frac{\partial B_x}{\partial z}\right)\hat{y} + \left(\frac{\partial B_y}{\partial x} - \frac{\partial B_x}{\partial y}\right)\hat{z}\right]. \quad (3.2)$$

Using a highly naive approach, lets look at two points at the magnetopause, the first of which is the sub-solar point in the equatorial plane. Since the Earth magnetic field is of order 10^3 times greater than the IMF we can assume that there is a magnetic vacuum around the magnetosphere. Then the gradient at the sub-solar point is directed along $-\hat{x}_{gsm}$ and the Earth magnetic field is essential directed along $\hat{z}$, equation 3.2 will then be reduced to

$$\mathbf{j} = \frac{1}{\mu_0}\left(\frac{\partial B_z}{\partial x}\right)\hat{y},$$

thus there is a current flowing in a Dusk-to-Dawn direction across the dayside magnetopause. The second is a arbitrary point at the top of the magnetotail,

again assuming a vacuum around the magnetosphere the gradient will be in the $-\hat{z}_{gsm}$-direction. Assuming that the magnetic field will be directed mostly in a $\hat{\mathbf{x}}$-direction, equation 3.2 reduces to

$$\mathbf{j} = -\frac{1}{\mu_0}\left(\frac{\partial B_x}{\partial z}\right)\hat{y},$$

here it is apperent that there is a current flowing around the magnetotail from the dusk side to the dawn side of the magnetosphere.

3.2 Magnetic reconnection

As stated before, one consequence of the MHD approximation for a plasma is the frozen in concept. This is valid only if the magnetic Reynolds number is large enough $R_m \gg 1$, if this is not the case, $R_m \approx 1$, it may break down. Looking at equation 2.10 we can conclude that this happens if the length scale, velocity or conductivity becomes small. A direct consequence of the frozen in concept is that a thin boundary is formed between different plasma regions. Within such a boundary the length scales are small and thus the frozen in concept may locally break down. This would then allow for particles from different plasmas to mix and thus exchange energy. The theory of where and how this break down occurs are very complex thus we are considering a simplified model of this hereon called the *antiparallel reconnection model*. In the antiparallel reconnection model we assume that reconnection may occur wherever the magnetic field lines are directed anti parallel to each other, see figure 3.3.

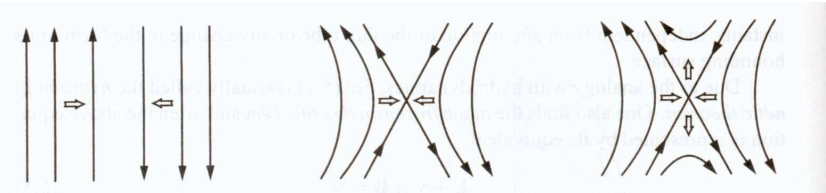

Figure 3.3: The stages in a reconnection event

This is what is happening at the magnetopause. In figure 3.4 the reconnection process is plotted for a strictly southwards IMF, $B_z < 0, B_y = 0$, in which case reconnection occurs between the magnetic fields embedded in the solar wind and the Earth's fields along the equatorial plane. The merged field lines will split into two, having one part attached to the IMF and one part to the Earth, this is the field lines marked by 2 in figure 3.4. These field lines will then get dragged down-tail by the solar wind (lines 3 - 6). At the night side end of the magnetosphere, two open field lines reconnect and forms a newly closed geomagnetic field line (line 7) and a purely interplanetary field line (line 8), at the same time transporting plasma towards Earth.

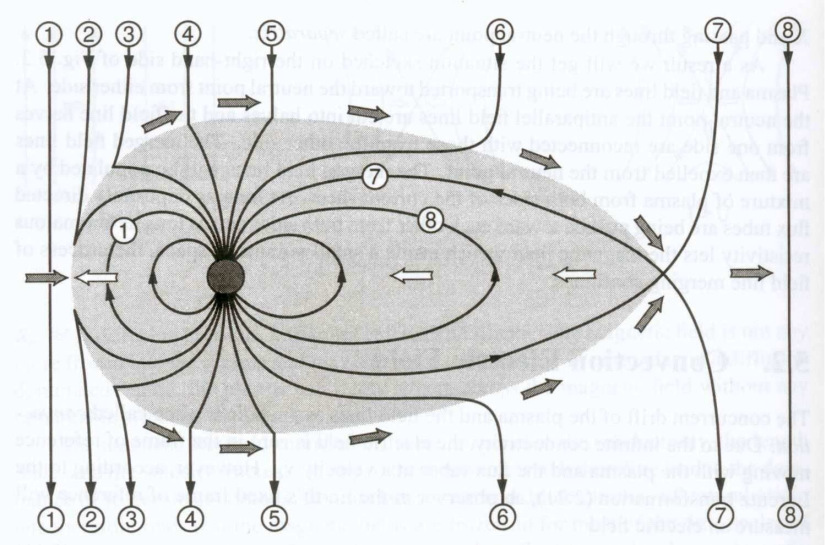

Figure 3.4: Field line merging and reconnecting at the magnetopause

The reconnection zone will be shifted according to the magnetic field components in the IMF, see [5] for a thorough discussion about this. Very simplistic we can say that a y-component will rotate the location in the YZ-plane and that a northward directed IMF, $z > 0$, will shift the location towards higher latitudes.

3.3 Energy flux equations

Using the ideas presented in this chapter up until this point it is possible to construct a model of how and most importantly where the energy transfer between the IMF and magnetosphere occurs. The total force (magnetic and electric) on a particle with charge q is given by the Lorentz force

$$\mathbf{F} = q(\mathbf{E} + \mathbf{v} \times \mathbf{B}). \tag{3.3}$$

Let $d\mathbf{F}$ denote the force on the charges in the volume dr and using equation 3.3 we get

$$d\mathbf{F} = (\rho_f \mathbf{E} + \mathbf{J}_f \times \mathbf{B})dr,$$

then the force per unit volume $\mathbf{f}_v$ can be expressed as

$$\mathbf{f}_v = \frac{d\mathbf{F}}{dr} = \rho_f \mathbf{E} + \mathbf{J}_f \times \mathbf{B},$$

and the total force on a volume V is then

$$\mathbf{F} = \int_V \mathbf{f}_v dr = \int_V (\rho_f \mathbf{E} + \mathbf{J}_f \times \mathbf{B})dr. \tag{3.4}$$

Using equations (2.1) and (2.4) to express $\mathbf{f}_v$ yields

$$\mathbf{f}_v = \epsilon_0 \mathbf{E}(\nabla \cdot \mathbf{E}) + \frac{1}{\mu_0}(\nabla \times \mathbf{B}) \times \mathbf{B} - \epsilon_0 \frac{\partial \mathbf{E}}{\partial t} \times \mathbf{B}$$

to increase symmetry, lets add zero in the form, again using Maxwell's equations,

$$-\epsilon_0 \mathbf{E} \times \frac{\partial \mathbf{B}}{\partial t} - \epsilon_0 \mathbf{E} \times (\nabla \times \mathbf{E}) + \frac{1}{\mu_0} \mathbf{B}(\nabla \cdot \mathbf{B}) = 0,$$

which yields

$$\mathbf{f}_v + \epsilon_0 \frac{\partial}{\partial t}(\mathbf{E} \times \mathbf{B}) = \epsilon_0 \left[\mathbf{E}(\nabla \cdot \mathbf{E}) - \mathbf{E} \times (\nabla \times \mathbf{E})\right] + \frac{1}{\mu_0} \left[\mathbf{B}(\nabla \cdot \mathbf{B}) - \mathbf{B} \times (\nabla \times \mathbf{B})\right]. \quad (3.5)$$

The right hand side of equation 3.5 is called Maxwell's stress tensor.

Equation 3.5 can be greatly simplified in a MHD plasma by rewriting equation 2.6 as

$$\mathbf{E} = -\mathbf{v} \times \mathbf{B} \Rightarrow \frac{E}{B} = v \sin \varphi \quad (3.6)$$

where φ is the angle between $\mathbf{v}$ and $\mathbf{B}$. The quota between the electric and magetic energy in an ideal MHD plasma is given by

$$\frac{W_e}{W_b} = \frac{\epsilon_0 \mathbf{E^2}/2}{\mathbf{B}^2/2\mu_0} = \epsilon_0 \mu_0 \left(\frac{\mathbf{E}}{\mathbf{B}}\right)^2. \quad (3.7)$$

Expressing the quota using equation 3.6 we get that the ratio is given by

$$\epsilon_0 \mu_0 v^2 \sin^2 \varphi = \frac{1}{c^2} v^2 \sin^2 \varphi < \frac{v^2}{c^2} \ll 1 \quad (3.8)$$

The gradient of the electric field can be large only on small scale length of the order of the Debye length. On larger scale length the electric term in Maxwell's stress tensor can be neglected compared to the magnetic term. Therefore we can neglect the first part of equation 3.5 and express $\mathbf{f}_v$ as

$$\mathbf{f}_v = \frac{1}{\mu_0} \left[\mathbf{B}(\nabla \cdot \mathbf{B}) - \mathbf{B} \times (\nabla \times \mathbf{B})\right],$$

which, using tensor notation, can be written as

$$\mathbf{f}_v = \nabla \cdot T_{ij}. \quad (3.9)$$

T_{ij} is called Maxwell's magnetic stress tensor and is given by

$$T_{ij} = \frac{1}{\mu_0}(B_i B_j - \frac{1}{2}\delta_{ij} B^2) \quad (3.10)$$

where δ_{ij} is the Kronecker delta and $\mu_0 = 4\pi 10^{-7}$ Vs/Am.

Using equation (3.9) its possible to rewrite equation (3.4) as

$$\mathbf{F} = \int_V \nabla \cdot \mathbf{T} d\mathbf{r}. \quad (3.11)$$

The total power trough the magnetopause is given by

$$U(W) = \mathbf{F} \cdot \mathbf{v} \quad (3.12)$$

where $\mathbf{v}$ is the magnetosheath velocity. Using equation (3.11) this becomes

$$U(W) = \int_V (\nabla \cdot \mathbf{T}) \cdot \mathbf{v} d\mathbf{r} \Rightarrow U(W) = \int_A dA \int_n (\nabla \cdot \mathbf{T}) \cdot \mathbf{v_t} dn$$

where in the last step there has been assumed that there exists a pressure balance across the magnetopause, thus we neglect all but the tangential components of the magnetosheath velocity. Using the definition of Maxwell magnetic stress tensor, equation (3.10), the expression can be simplified to

$$\nabla \cdot \mathbf{T} = \frac{1}{\mu_0}(\mathbf{B} \cdot \nabla) \cdot \mathbf{B} - \nabla \left(\frac{B^2}{2\mu_0} \right) = \nabla \cdot \mathbf{T}_s - \nabla \left(\frac{B^2}{2\mu_0} \right) = \frac{1}{\mu_0}(\nabla \times \mathbf{B}) \times \mathbf{B} = \mathbf{j} \times \mathbf{B}$$

where equation 2.1 has been used. Using this result and noting that $dn = v_{mp} dt$, where v_{mp} is the magnetopause velocity, the total power can be expressed as

$$U(W) = \int_A dA \underbrace{\int_t (j \times B) \cdot \mathbf{v_t} v_{mp} dt}_{Q} \tag{3.13}$$

and Q is the local power that we want to investigate in this study. Looking at equation 3.12 we can see that for an energy transfer to occur then $\mathbf{F}$ and $\mathbf{v}$ has to have parallel components. When reconnection occurs at the dayside magnetopause energy will be transferred from the magnetic field in the solar wind to the particles in the magnetopause. This effect can naively be explained by thinking of the newly connected magnetic field lines as a rubber band. A rubber band always strives for the minimization of the total contained energy and is accelerated in the direction where this state can be achieved. So will the connected field lines, looking at figure 3.4 this acceleration will occur at the region in between the reconnection zone and the field line marked by 4. Since the particles in the magnetopause are stuck to the magnetic field lines they too will be accelerated in this process and gain energy. Due to this acceleration the force $\mathbf{F}$ in this zone will have small components parallel to the solar wind and the power input from these components will be neglectable when compared to the power output due to the accelerations of particles. Returning to figure 3.4 but this time looking at the zone marked by field lines 4 to 7. In this zone the rubber band effect of the connected field lines will try to reduce the night side motion of magnetic fields. This will cause a force $\mathbf{F}$ directed directly anti parallel to the solar wind thus yielding a energy input. The different regions and their expected energy fluxes are marked in figure 3.5 for a southward IMF. A positive energy flux, i.e. power flowing out of the magnetosphere, corresponds to particles gaining energy from the magnetic field, this situation is also called a load and is marked with red in the figure. A negative flux, i.e. power flowing in to the magnetosphere, corresponds to that the magnetic field gains energy from the particles, this situation is called a generator and is marked with green in the figure.

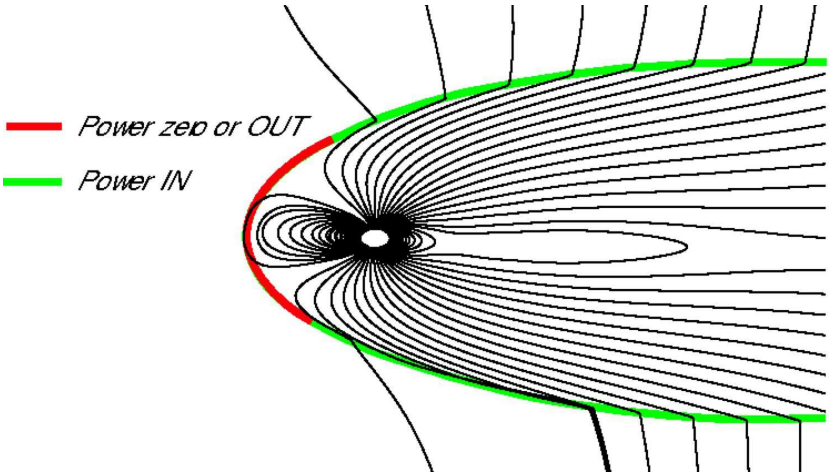

Figure 3.5: Theoretical regions of energy input and output on the magnetopause with a southward directed IMF

For a northward directed IMF the situation will be different, then reconnection occurs at high latitudes near field line 4 in figure 3.4. This means that there should be a close to zero energy flux at the dayside. Also at most of the nightside there will be a zero energy flux except in the area close to the reconnection zone, were there of course will be a positive energy flux. Also at the nightside there will be a energy input in the area where the newly connected fieldlines get dragged over the magnetopause.

Chapter 4

Instrumentation and techniques

This chapter is devoted to the different instruments, Advanced Composition Explorer and Cluster, used to gather the necessary data. Also the different techniques, timing, minimum variance analysis and the curlometer method, used are described with the theory behind them derived.

4.1 ACE

Receding at the L1 Lagrangian point (Sun-Earth gravitational equilibrium), see figure 4.1 the Advanced Composition Explorer (ACE) monitors the solar wind and the interplanetary magnetic field.

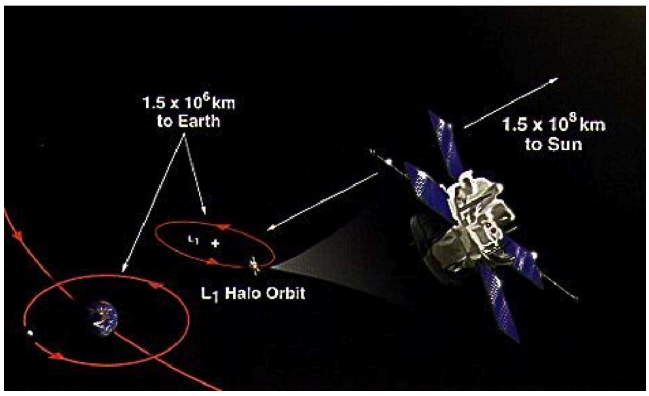

Figure 4.1: ACE satellite and its place in space (from [9]).

Using ACE it's possible to obtain high resolution, sample frequency of 0.2 Hz, solar wind data. One problem with this data is that for average solar wind properties the traveling time to reach Earth from L1 is about 40 minutes, so it has to be shifted accordingly to make it possible to compare measurements from ACE with measurements at the Earth. This shifting can be accomplished by two different methods. The first is called Parallel shifting, in this method

one simply average the solar wind speed using previously sampled data and calculate the time delay by knowing the distance from ACE to Earth. It has been shown, see [7], that the uncertainties using Parallel shifting are quite high, up to 20 minutes. The second method is a more sophisticated method using the minimum variance technique developed by Weimer[7]. This method reduce the uncertainties to about 5 minutes.

4.2 Cluster

The multi-spacecraft mission Cluster, figure 4.2(a), was launched in 2000 and constitutes of four spacecrafts flying in a tetrahedral formation, see 4.2(b), in an eccentric polar orbit measuring, among other things, the fluctuations in magnetic and electric fields. The unique geometry of Cluster provides the means to study the energy flows in the coupled Sun-Earth system. The instrumentation used in this report is the *Cluster Ion Spectrometry* (CIS) for ion speed and the *Fluxgate Magnetometer* (FGM) for magnetic field data.

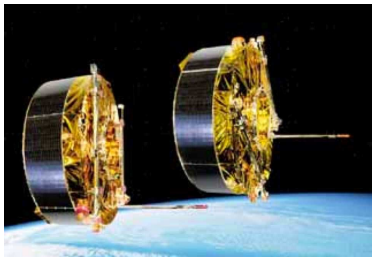

(a) Two of the cluster satellites depicted in space.

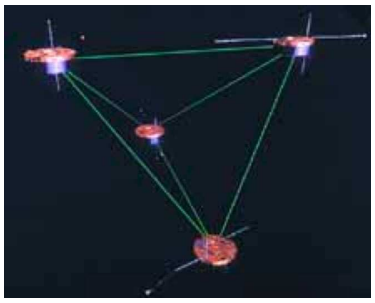

(b) A typical cluster tetrahedron formation.

Figure 4.2: Cluster pictures and the tetrahedral formation (from [2]).

Thus, it is possible to estimate local measurements of the magnetopause velocity $\mathbf{v}_{mp}$, magnetopause normal $\hat{\mathbf{n}}$ and current $\mathbf{j}$ during a magnetopause crossing, it is also possible to calculate $\nabla \cdot \mathbf{T_s}$. These four parameters are the necessary parameters for estimating the energy transfer between the solar wind and the magnetosphere, see equation 3.13. To estimate these quantities three different methods were used, *4-spacecraft timing* and *minimum variance* to analyze discontinuities and the *curlometer technique* used to approximate the curl of the magnetic field.

4.2.1 Curlometer technique

The curlometer technique is used to approximate the curl in a magnetic field, $\nabla \times \mathbf{B}$ using 4-point measurements. Using this technique in combination with Ampere's law (equation 2.1) it is possible to calculate the local current $\mathbf{j}$ flowing around the magnetopause. By assuming that the electric field is constant inside the tetrahedron formed by the four cluster spacecraft Ampere's law is reduced to

$$\nabla \times \mathbf{B} = \mu_0 \mathbf{j}$$

from which the current is easily obtained. The curlometer technique employs a difference estimate of $\nabla \times \mathbf{B}$ as follows

$$\mu_0 \mathbf{j}_{av} \cdot (\mathbf{r}_{1\alpha} \times \mathbf{r}_{1\beta}) = \Delta \mathbf{B}_{1\alpha} \cdot \mathbf{r}_{1\beta} - \Delta \mathbf{B}_{1\beta} \cdot \mathbf{r}_{1\alpha}$$

As a quality measure of this technique the divergence of the magnetic field, $\nabla \cdot \mathbf{B}$ can be studied. According to Maxwell's equations (equation 2.3), this should be zero. Any result other than this is caused by errors in either measurements, linear interpolations between the satellites or due to inner structures in the current sheet. Normalizing this with respect to the current in the sheet we take as a quality measure the quota $\frac{\nabla \cdot \mathbf{B}}{|\nabla \times \mathbf{B}|}$.

The curlometer technique requires a sufficiently thick magnetopause since the spacecraft separation must be smaller than the thickness of the current sheet. Furthermore the planarity, which is a measure of the tetrahedron formation, must be small to reduce the error of the method. A planarity close to unity means that all four satellites lies in the same plane whilst the geometry is a tetrahedron if the planarity is close to zero.

4.2.2 4-spacecraft timing

If multiple spacecraft crosses the same boundary, their relative positions and timings can be used to acquire the boundary speed and normal. This due to the fact that

$$(\mathbf{V} t_{\alpha\beta}) \cdot \hat{\mathbf{n}} = \mathbf{r}_{\alpha\beta} \cdot \hat{\mathbf{n}},$$

where $\mathbf{r}_{\alpha\beta}$ is the separation vector between two spacecraft and $t_{\alpha\beta}$ the time difference between this pair for a particular boundary. This is easily extended to four spacecrafts which yields the following system of equations

$$\begin{pmatrix} \mathbf{r}_{12} \\ \mathbf{r}_{13} \\ \mathbf{r}_{14} \end{pmatrix} \cdot \frac{1}{\mathbf{V} \cdot \hat{\mathbf{n}}} \begin{pmatrix} \mathbf{n}_X \\ \mathbf{n}_Y \\ \mathbf{n}_Z \end{pmatrix} = \begin{pmatrix} \mathbf{t}_{12} \\ \mathbf{t}_{13} \\ \mathbf{t}_{14} \end{pmatrix}$$

The problem with this method is that it requires a small spacecraft separation, due to changes in the boundary properties. Also the method assumes that the boundary is planar, a bump in the boundary may lead to totally misleading results.

4.2.3 Minimum variance analysis

The purpose of the minimum variance analysis (MVA) is to find, from single spacecraft data, an estimator for the direction normal to an approximately one-dimensional current layer.

If we assume that the current layer is ideal one dimensional (i.e. $\partial/\partial x = 0$, $\partial/\partial y = 0$), then the only remaining component of the divergence of $\mathbf{B}$ (equation 2.3) is

$$\nabla \cdot \mathbf{B} = \frac{\partial B_z}{\partial z} = 0,$$

thus B_z is independent of z, here the z-axis is pointing in the direction of the sought after $\hat{\mathbf{n}}$. Then it follows from Faraday's law (equation 2.2) that B_z must be time independent, $\partial B_z/\partial t = 0$, and the spacecraft should observe a constant

value of B_z during the crossing. In this ideal event only three different measurements of the magnetic field, $\mathbf{B}^{(1)}$, $\mathbf{B}^{(2)}$, and $\mathbf{B}^{(3)}$, are needed to determine $\hat{\mathbf{n}}$. Here $\mathbf{B}^{(1)}$ is measured just before the crossing, $\mathbf{B}^{(2)}$ during the crossing and $\mathbf{B}^{(3)}$ after the crossing. Since B_z is independent of both time and space then

$$\mathbf{B}^{(1)} \cdot \hat{\mathbf{n}} = \mathbf{B}^{(2)} \cdot \hat{\mathbf{n}} = \mathbf{B}^{(3)} \cdot \hat{\mathbf{n}}$$

thus the vectors $\left(\mathbf{B}^{(1)} - \mathbf{B}^{(2)}\right)$ and $\left(\mathbf{B}^{(2)} - \mathbf{B}^{(3)}\right)$ are tangential to the current layer. Thus their cross product is pointing along $\hat{\mathbf{n}}$. So the final expression for the normalized current layer normal would then become

$$\hat{\mathbf{n}} = \frac{\left(\mathbf{B}^{(1)} - \mathbf{B}^{(2)}\right) \times \left(\mathbf{B}^{(2)} - \mathbf{B}^{(3)}\right)}{\left|\left(\mathbf{B}^{(1)} - \mathbf{B}^{(2)}\right) \times \left(\mathbf{B}^{(2)} - \mathbf{B}^{(3)}\right)\right|} \tag{4.1}$$

This is just the basic theory behind the method. In reality the current sheets almost always has a internal 3D structure, causing fluctuations of the $\mathbf{B}$ field during the crossing. The best approximation to the normal is aquired using a statistical method and a set of measured values $\left\{\mathbf{B}^{(m)}\right\}\, m = 1, 2, 3, \ldots, M$ sampled during the crossing. An estimation of $\hat{\mathbf{n}}$ is the direction in which $\left\{\mathbf{B}^{(m)} \cdot \hat{\mathbf{n}}\right\}\, m = 1, 2, 3, \ldots, M$ has minimum variance. In other words the normal to the sheet is found by minimizing

$$\sigma^2 = \frac{1}{M} \sum_{m=1}^{M} \left| \left(\mathbf{B}^{(m)} - \langle \mathbf{B} \rangle\right) \cdot \hat{\mathbf{n}} \right|^2$$

where $\langle \mathbf{B} \rangle$ is the average of the measured set and where the minimisation is subject to the normalization constraint $|\hat{\mathbf{n}}|^2 = 1$. This minimization problem can be transformed into the following system of homogeneous equations

$$\begin{aligned}
\frac{\partial}{\partial n_X}\left(\sigma^2 - \lambda\left(|\hat{\mathbf{n}}|^2 - 1\right)\right) &= 0 \\
\frac{\partial}{\partial n_Y}\left(\sigma^2 - \lambda\left(|\hat{\mathbf{n}}|^2 - 1\right)\right) &= 0 \\
\frac{\partial}{\partial n_Z}\left(\sigma^2 - \lambda\left(|\hat{\mathbf{n}}|^2 - 1\right)\right) &= 0
\end{aligned}$$

using a Lagrange multiplier λ, where (n_X, n_Y, n_Z) is the components of $\hat{\mathbf{n}}$ along the GSM coordinates (X, Y, Z). This system reduces to a eigenvalue problem after the differentiations have been performed,

$$\sum_{\nu=1}^{3} M^B_{\mu\nu} n_\nu = \lambda n_\mu \tag{4.2}$$

where $\mu, \nu = 1, 2, 3$ is the components along (X, Y, Z) and

$$M^B_{\mu\nu} \equiv \langle B_\mu B_\nu \rangle - \langle B_\mu \rangle \langle B_\nu \rangle$$

is what's called a magnetic variance matrix. Solving equation 4.2 yields a set of eigenvectors, $\{l, m, n\}$ and their corresponding eigenvalues $\{\lambda_1, \lambda_2, \lambda_3\}$. The eigenvector corresponding to the smallest eigenvalue is the sought approximation to $\hat{\mathbf{n}}$, the other two, $\hat{\mathbf{m}}$ and $\hat{\mathbf{l}}$, will lay in the magnetopause plane. Of course these vectors are linearly independent and hence constitutes a coordinate system, hereon called the *nml*-coordinates.

4.3 Theoretical model

To compare the acquired normals from both the timing and the MVA we created a computer program using the Shue et al.[6] magnetopause model

$$r = r_0 \left(\frac{2}{1 + \cos\theta} \right)^{\alpha},$$

where r is radial distance and θ is solar zenith angle. The two parameters r_0 and α represents the standoff distance and the level of tail flaring respectively defined as

$$r_0 = 10.22 + 1.29 \tanh 0.184(B_z + 8.14))D_p^{\frac{-1}{6.6}}$$

$$\alpha = (0.58 - 0.007B_z)(1 + 0.024 \log D_p)$$

where B_z is the z_{gsm} component of the IMF and D_p the solar wind dynamic pressure defined as

$$D_p = 1.95 * 10^{-6} * nv_{sw}^2,$$

here v_{sw} is the solar wind velocity and n is the solar wind density. Using this model we could calculate the theoretical normal of the closest point to the Cluster satellites on the magnetopause. The direction of this theoretical normal could then be compared to the measured normals as a quality check of the estimations. In figure 4.3 we see the Shue. et. al. calculated magnetopause from a location at the night side magnetosphere, looking towards the sun. The magnetopause crossing occurred inside the black square. Zooming in on this region, we see the location of the first cluster satellite, C1, marked by a 1, further more we see the calculated nearest point marked by a red square at the magnetopause. Also present in the figure is the calculated normal marked by a blue line.

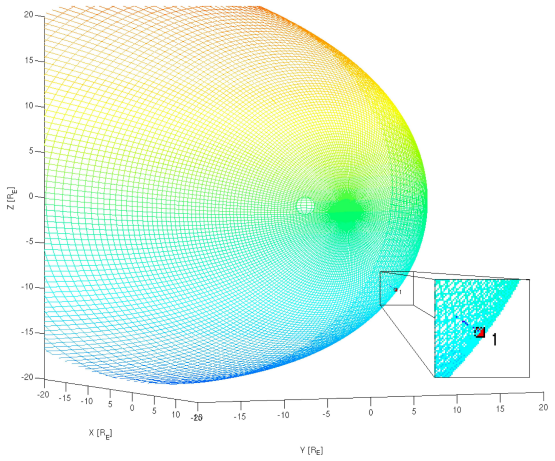

Figure 4.3: The Shue et. al. magnetopause model with the location of one of the Cluster satellites and the closest point on the magnetopause to this satellite marked. Also the normal is plotted as the blue line.

Chapter 5

Results

In this chapter the theory from the previous four chapters will be combined and applied to the problem. The chapter starts by a short discussion around the measurements and data collection. This is followed by a section where the actual results are presented. Lastly there is a discussion around the results.

5.1 Magnetopause identification and Cluster crossings

To find magnetopause crossings we started by using the Cluster quicklook webpage [3]. On this page it's easy to get a quick overview of the Cluster measurements over a long period of time. In figure 5.1 we see the data used in this step. If we look at panels 4 and 5 the magnetopause crossings are easily identified. Plotted in the panels are the ion and electron energy flux spectrograms respectively. Around 10 o'clock there is a sudden energy flux decrease in both panels at the same time the magnetic field strength, plotted in panel 1, around Cluster is decreased . This is a typical magnetopause crossing. Since we are coming from an area with high particle energy with large magnetic field magnitude to an area with low energy and with a lower magnetic field magnitude we can draw the conclusion that this crossing occurred from the magnetosheath to the magnetosphere.

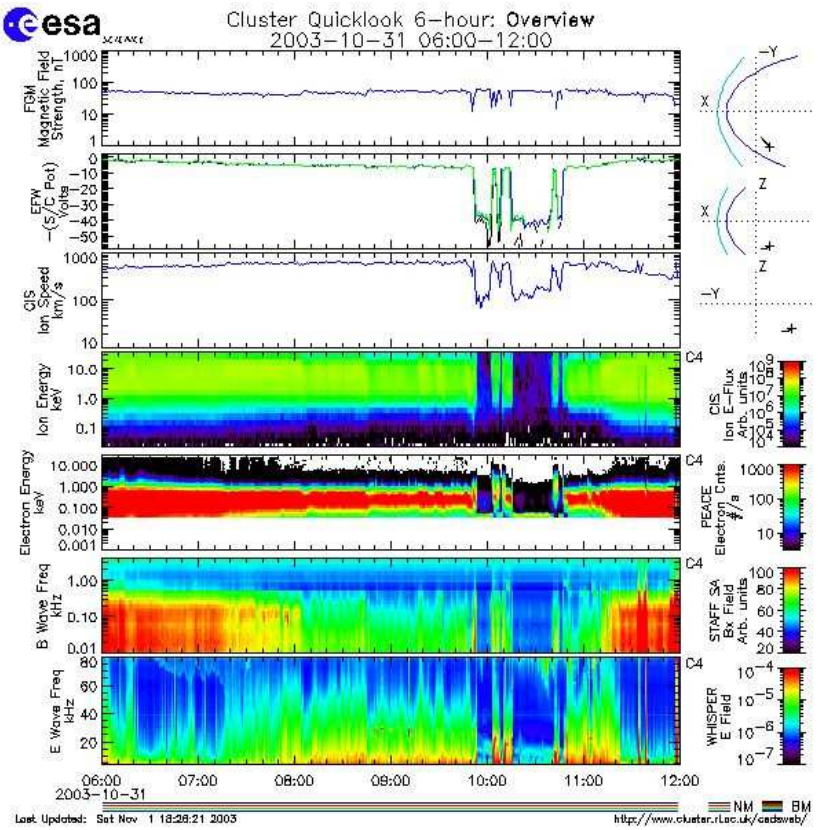

Figure 5.1: The plots used to identify potential crossings. Data downloaded from [3].

We searched the Cluster database for such crossings during the time periods that fulfilled our criteria (see section 5.2). The data for each individual crossing were then downloaded from IRFUs local data repository with a much higher time resolution than in the quicklook plots.

5.2 Statistics

Due to the limitations of the techniques we use in the analysis of the data we required that the separation of the Cluster satellites were less than 600 km, which is the typical thickness of the magnetopause. This requirement narrowed the scope of the total crossings to 2001, two month in the beginning of 2002, then a couple of month at the end of 2003 and the beginning of 2004. In figure 5.2 the planned Cluster separation are plotted, also plotted are the location of Cluster, if in the tail or cusp. This scope was further narrowed when the planarity requirement associated with the curlometer technique was introduced.

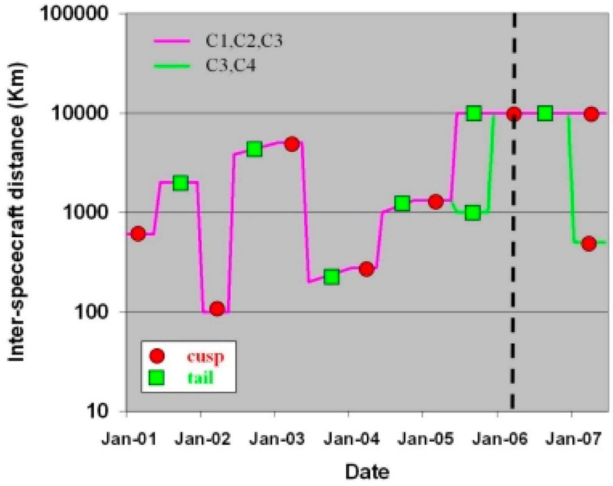

Figure 5.2: Cluster satellites planned separation

Most of the downloaded high resolution data revealed crossings that wasn't apparent using the Cluster quicklook webpage. Many of the crossings were actually multiple crossings, which means that as the Cluster satellites move, the motion of the magnetopause makes the boundary pass the satellites several times. In figure 5.3(a) the magnetic fields are plotted during a single crossing, the blue field marks the crossing. To the left of this field we see that all components B_{xyz} are quite stable at -40 nT, 20 nT and -5 nT respectively. Then suddenly, B_x rises, maximizing at around $22 - 23$ nT, at the same time B_y plunges to around -20 nT. To the right of the blue field all three components displays a chaotic behavior oscillating wildly around $B_{xyz} = 0$ nT. This is a typical crossing where Cluster comes from inside the magnetosphere (to the left of the blue field), crosses the magnetopause (the blue field) and continues through the magnetosheath (to the right of the blue field), actually this is crossing # 10 in table 5.1. If we instead look at figure 5.3(b) we see that first we have an apparent crossing from the magnetosphere to the magnetosheath. This is the first blue field. Then suddenly the magnitude of B_x increases and all components stabilizes, this is a crossing from the magnetosheath into the magnetosphere and is marked by the second blue field. Soon after this second crossing we can see that the magnitude decreases and the oscillations resumes, thus Cluster is out in the magnetosheath again, this is the third blue field. This behavior continues and in total Cluster crosses the magnetopause seven times. The four marked fields are the only crossings where good normals were acquired, these are the crossings # 11-14 in table 5.1. These multiple crossings are important because they allows us to examine the changes in energy flux in a small area of the magnetopause. In total we were able to isolate two such multiple crossings (id #: 5-8 and 11-14 in table 5.1) .

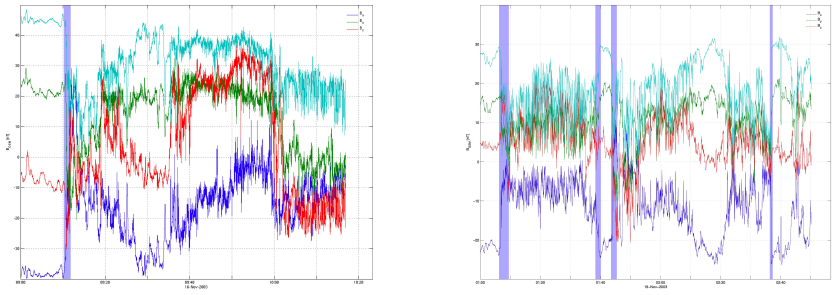

(a) One single magnetopause crossing

(b) Multiple magnetopause crossings, event # 12-15

Figure 5.3: The two different types of magnetopause crossings

Unfortunately did the problems associated with the analysis techniques, i.e. the thickness of the magnetopause, force us to remove a great deal of all the crossings. In the end we were able to isolate 15 different magnetopause crossings. all but one on the night side, where the confidence in the MVA is high enough and the timing, MVA and model normals are consistent. These crossings are presented in table 5.1 below.

#	Date	Start	Stop	B_y	B_z	C1 coord (GSM)
1	02-03-14	01:04:44	01:07:40	2.67	4.94	$(7.9, -3.0, 8.0)$
2	03-10-30	19:49:00	19:50:20	-8.6	-25.4	$(-9.6, 14.6, -7.9)$
3	03-10-31	10:40:00	10:41:10	-4.04	16.29	$(-2.6, 4.0, -14.0)$
4	03-11-04	06:29:03	06:30:35	-3.24	0.8	$(-9.8, 14.3, -6.8)$
5	03-11-04	19:14:20	19:18:12	-3.18	1.3	$(-6.4, 14.2, -10.4)$
6	03-11-04	19:51:04	19:52:15	-2.99	0.63	$(-6.2, 14.1, -10.3)$
7	03-11-04	19:57:41	19:59:40	-3.44	-0.94	$(-6.1, 14.1, -10.3)$
8	03-11-04	20:31:24	20:33:25	-0.79	1.59	$(-5.7, 14.0, -10.3)$
9	03-11-07	07:32:04	07:35:42	-3.09	2.62	$(-4.4, 9.7, -14.3)$
10	03-11-16	09:09:45	09:12:28	0.46	1.9	$(-5.2, 15.0, -11.0)$
11	03-11-19	01:06:14	01:09:29	2.59	0.54	$(-2.5, 16.5, -8.6)$
12	03-11-19	01:38:17	01:40:06	1.68	0.86	$(-2.3, 16.2, -9.1)$
13	03-11-19	01:43:29	01:45:26	0.6	0.99	$(-2.3, 16.1, -9.2)$
14	03-11-19	02:36:31	02:37:18	1.28	0.23	$(-2.0, 15.3, -10.1)$
15	03-11-30	03:30:40	03:33:40	-4.66	-7.33	$(-3.1, 15.9, 1.6)$

Table 5.1: The magnetopause crossings used in this report. # is a unique identification number, Date is the date when the crossing occurred, Start is the start time of the crossing in the format (hh:mm:ss) and Stop is the stop time of the crossing in the same format. B_y, B_z is the y and z component of the IMF in GSM coordinates, C1 coord is the GSM coordinates of the Cluster satellite C1 at the time of the crossing.

5.3 Data analysis

The timing and minimum variance measurements were made by hand, using tools for MATLAB developed at IRFU, see figure 5.4(a) for the MVA GUI and

5.4(b) for the timing.

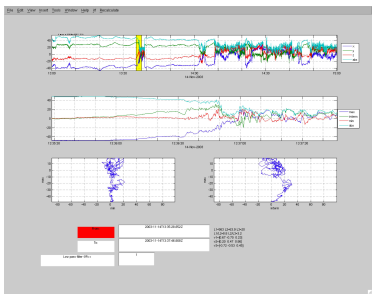

(a) The GUI used for minimum variance analysis.

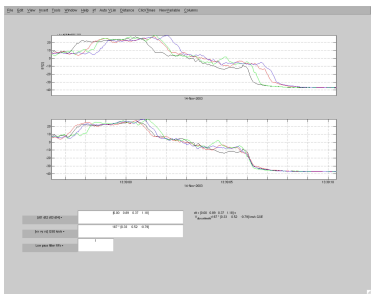

(b) The GUI used for timing.

Figure 5.4: The different GUIs.

One problem with this hands-on technique is that it's often hard to determine where the magnetopause crossing starts and ends. This can be realised by looking at figure 5.3(b). In the figure only four crossing are marked, but there are strong indications that three more exists, two between the last two blue lines and one after the last line. For these three crossing there exists no clear start and end of the crossing and thus the MVA can't be performed. A too long data interval may result in high accuracy MVA normals but completely different normals when using timing. On the other hand when using a short interval it is easy to get timing normals consistent with model normals, but the MVA yields normals with too low of a confidence to trust. What's worse is that even if both normals are consistent the energy calculations may yield ambiguous results if the interval is too long with respect to the thickness of the magnetopause.

After reliable normals are acquired the energy flux according to equation 3.13 can be calculated. A MATLAB software was developed to help during this final stage of the analysis, see figure 5.5. The software is described in detail in Appendix A.1.

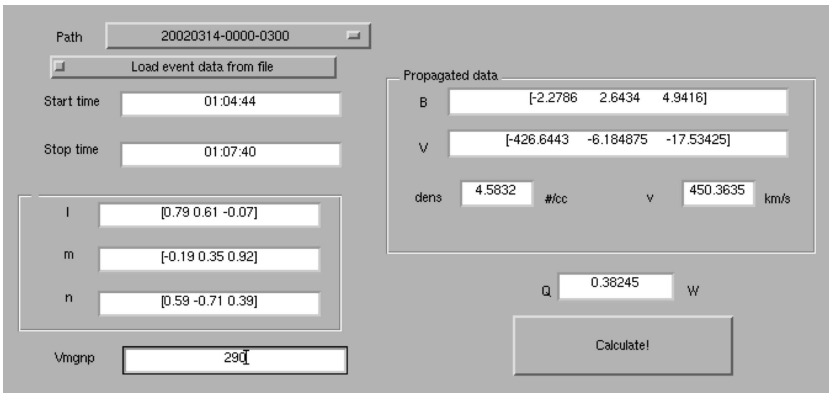

Figure 5.5: The GUI developed to help with the data analysis.

5.4 Results

As mentioned before it is possible to divide the results into two groups, those with positive power and those with negative, the first group are called load regions, the latter called generator regions. The positive power in a load corresponds to energy transferred from the magnetic field to particles, a generator on the other hand corresponds to energy transferred from particles to the magnetic field.

5.4.1 Example of a load

In figure 5.6 the output from our energy flux program is presented, this is for crossing #7. In panel 5 we see that during the magnetopause crossing the power is steadily increasing. In panel 2 we also see the characteristic reconnection jets which indicates that the crossing occurred near the reconnection zone thus a load is expected according to the theory.

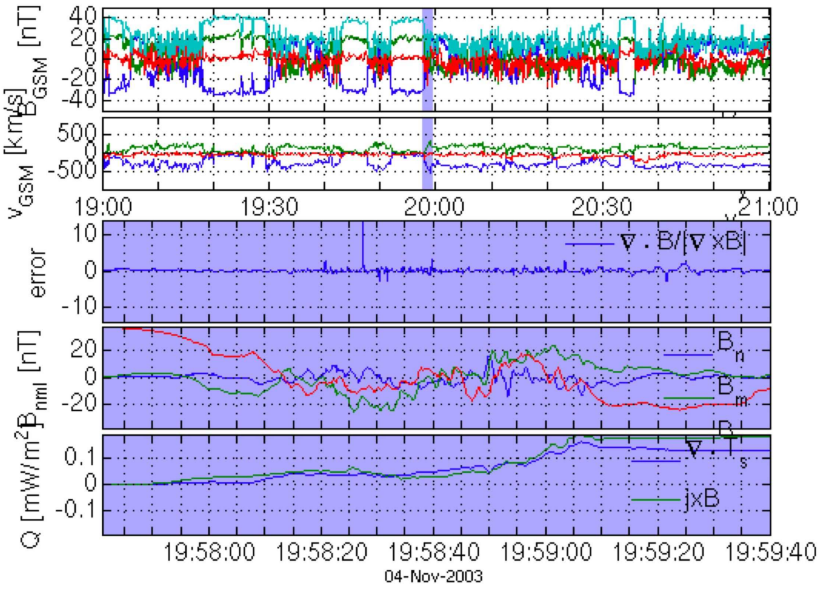

Figure 5.6: The output plot for event #7, in this case we have a load region, $Q > 0$, on the magnetopause.

5.4.2 Example of a generator

In figure 5.7 the output from our energy flux program for crossing #14 is presented. We see no jets in panel 2 this indicates that we are nowhere near the reconnection zone and that we would expect a negative or close to zero power. In panel 5 we see that the power is steadily decreasing during the crossing thus this is a generator and it is consistent with the theory.

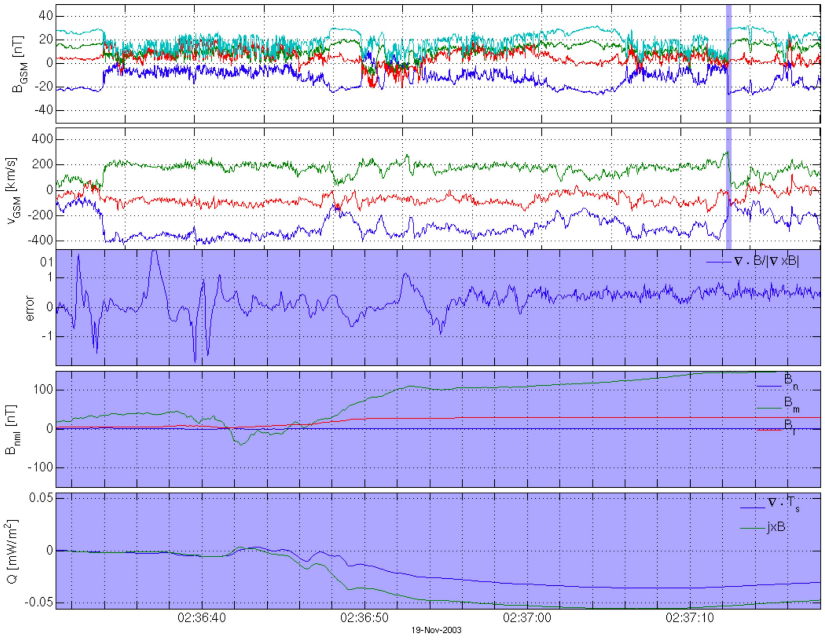

Figure 5.7: The output plot, in this case we have a generator region, $Q < 0$, on the magnetopause.

5.4.3 Statistical results

In table 5.2 all the events with their calculated normals, both using timing and the minimum variance techniques, and respective local energy flux is presented.

#	$\hat{\mathbf{n}}_{timing}$	$\hat{\mathbf{n}}_{minvar}$	Q_{timing}	Q_{minvar}
1	$[0.67 \quad -0.39 \quad 0.63]$	$[0.59 \quad -0.71 \quad 0.39]$	0.368	0.405
2	$[-0.29 \quad -0.85 \quad 0.45]$	$[-0.52 \quad -0.82 \quad 0.24]$	-0.18	-0.25
3	$[-0.66 \quad -0.52 \quad 0.55]$	$[-0.66 \quad -0.45 \quad 0.61]$	0.0828	0.0822
4	$[-0.45 \quad 0.71 \quad 0.54]$	$[0.45 \quad 0.82 \quad 0.36]$	0.333	1.062
5	$[0.41 \quad 0.86 \quad -0.3]$	$[0.41 \quad 0.83 \quad -0.37]$	0.0402	0.04
6	$[0.4 \quad 0.83 \quad -0.38]$	$[-0.39 \quad -0.75 \quad 0.54]$	0.0087	0.0068
7	$[-0.62 \quad -0.66 \quad 0.43]$	$[0.51 \quad 0.81 \quad -0.29]$	0.135	0.131
8	$[0.26 \quad 0.86 \quad -0.45]$	$[-0.35 \quad -0.83 \quad 0.44]$	0.0058	0.006
9	$[-0.36 \quad -0.5 \quad 0.79]$	$[0.41 \quad 0.59 \quad -0.7]$	0.0507	0.058
10	$[-0.71 \quad -0.65 \quad 0.29]$	$[-0.62 \quad -0.77 \quad 0.18]$	-0.037	-0.04
11	$[-0.52 \quad -0.85 \quad 0.072]$	$[0.56 \quad 0.8 \quad -0.21]$	0.0407	0.0445
12	$[0.29 \quad 0.59 \quad -0.75]$	$[-0.49 \quad -0.87 \quad 0.03]$	0.0048	0.0437
13	$[-0.52 \quad -0.84 \quad 0.13]$	$[-0.65 \quad -0.76 \quad -0.02]$	0.0189	0.0159
14	$[0.16 \quad 0.52 \quad -0.84]$	$[0.15 \quad 0.48 \quad -0.87]$	-0.028	-0.0295
15	$[-0.6 \quad -0.8 \quad -0.041]$	$[-0.4 \quad -0.91 \quad -0.09]$	-0.031	0.0107

Table 5.2: The normals for each crossing, both from timing and from minimum variance, and the local energy flux.

In figure 5.8 we show the z-component of the IMF for all events plotted

versus the energy flux. The z-component of the IMF is the component that will have the greatest effect on the power input/output assuming the antiparallel reconnection model. When we have a southward IMF, i.e. when $B_z < 0$, reconnection will occur at the dayside magnetosphere. The newly connected IMF-magnetospheric magnetic field lines will then get dragged around the whole magnetotail. Looking at figure 3.4 we see this process occuring in a cross section of the magnetopause. This will actually occur in a similar manner all over the dayside magnetopause, this means that the magnetic tension forces that are vital for an power output will arise around the whole magnetotail. If on the otherhand we have an northward IMF, reconnection occur at high latitudes at the nightside magnetopause. This means that the newly connected field lines will be dragged only in a small area of the magnetopause and the power input/output occurs in a smaller part of it. The x- and y-component of the IMF will have the effect that it will shift the location of the reconnection zone. The y-component will shift it in the yz-plane and the x-component in the xz-plane, but it's always the sign of the z-component that determines whether it will be a dayside (southward) or nightside (northward) reconnection.

The colour coding represents the distance from the neutral sheet ($Z_{gsm} = 0$). The horizontal bars represents the span of energy flux when using either the normals yielded from timing or using the normals from MVA and are interpreted as error bars.

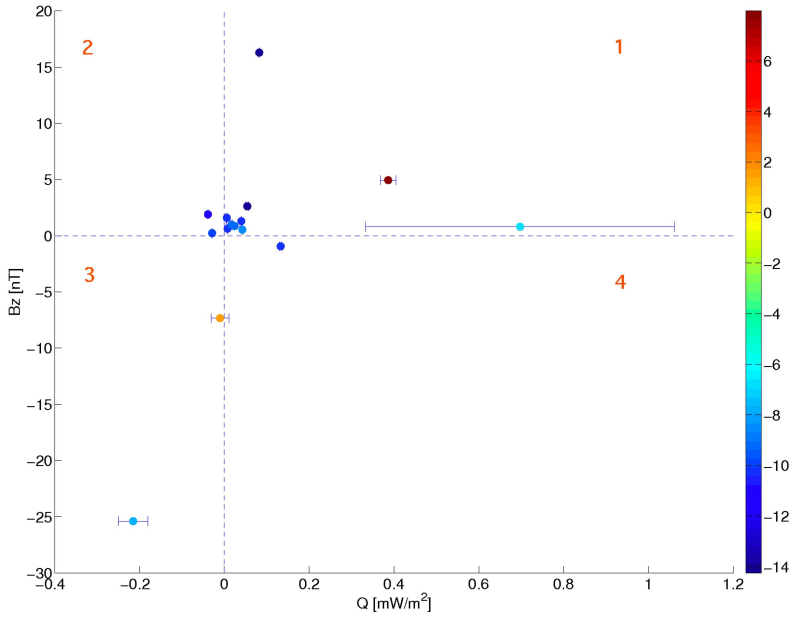

Figure 5.8: The dependence of energy flux versus the z-component of the IMF also shown are the numbering of the different quadrants.

5.5 Discussion

We can categorize the different quadrants in figure 5.8 into categories based on where the crossing occurred at the magnetopause. In quadrant 1 were we have a northward IMF and a positive energy flux thus according to the theory we should have events taking place at high latitudes here. High latitudes is indicated by the points being either dark blue or dark red, and looking at the figure we see that all points except one are. The light blue point with the huge error bar is in need of some explanation, that's event #4. Referring to table 5.2 we see that the normals from the MVA and timing measurements have different signs of the x-component. This is what gives the huge energy span. In table 5.1 we see that we have a dominating y-component of the IMF and Cluster is at low latitudes $(-9.8, 14.3, -6.8)$ Re. Looking at panel 2 in the energy plot of this event, figure 5.9, we see small indications of jets, but not nearly enough to contribute to such a big energy output. We have no explanation of this event at the current time, maybe it is a shift problem or maybe waves on the magnetopause contribute to the different normals.

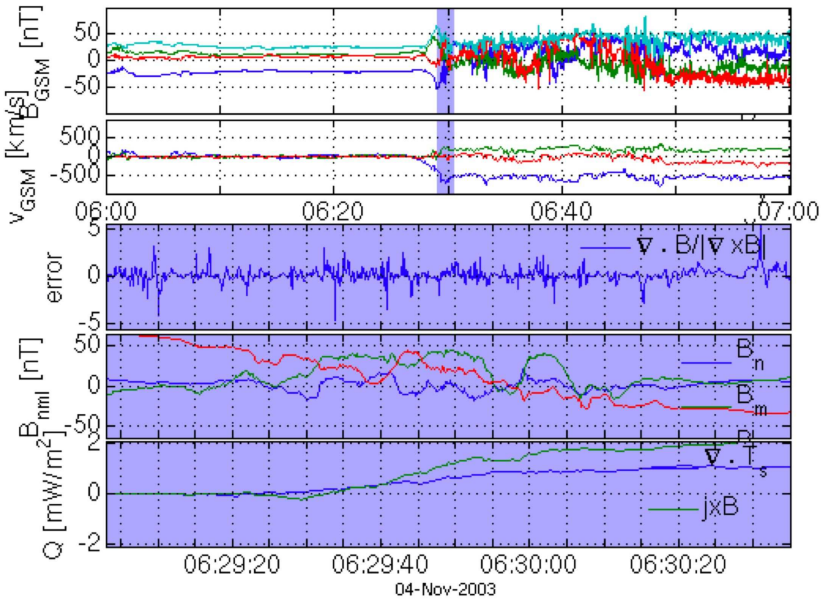

Figure 5.9: The output plot of event #4.

In quadrant 3 where the IMF is south and we have a negative energy flux we expect the events to take place at the tail. Looking at table 5.2 and table 5.1 we determine that the two events in this quadrant are #2 and #15 both of which occurred in the tail. Since the energy input will occur at the whole tail for a southward IMF it is interesting to notice how the colour changes as the energy flux decreases. Since only two points lay in this quadrant no real conclusions can be made but a trend can be seen. This trend is that as the crossings occur closer to the neutral sheet the power input is decreased. This can be seen in figure 5.8 since event #15 occurred closer to the neutral sheet (it

has a yellow colour) and have much less power input then does event #2 which occurred at higher latitudes. Of coarse the energy input is highly dependent of the magnitude of the IMF.

Events occurring in quadrant 2 are expected to have a dominating y-component in the IMF and to be at high latitudes. Again referring to tables 5.2 and 5.1 we see that the two events in this quadrant are #10 and #14. For event #14 we have a dominating y-component and it's consistent with the theory. Event #10 is also consistent with the theory but need more explanation since here the z-component is dominating. For this event we have a northward IMF and Cluster is at $(-5.18, 15.01, -10.99)$, thus in the tail. Looking at panel 1 in figure 5.10 we can conclude that this position is consistent with the direction of the magnetic field. Reconnection will occur at the Dawn-side below the equatorial plane and at the Dusk-side above. This means that cluster is far away from the reconnection zone and as expected we see no jets in panel 2 during the crossing. Also looking at particle velocity we find that during the crossing they are about the same as the solar wind. This implies that no field lines get dragged over the area, thus there should be no energy flux. But we calculate a negative flux, see panel 6.

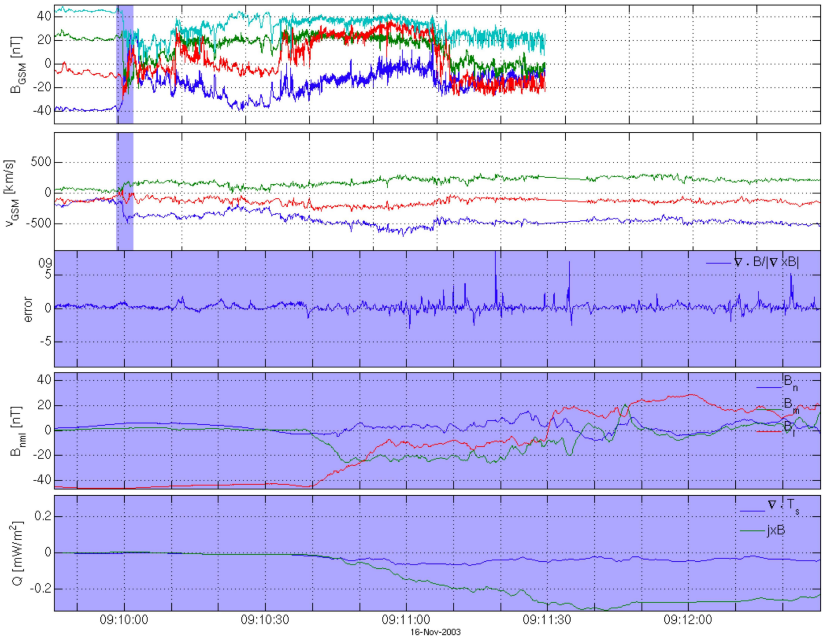

Figure 5.10: The output plot of event #10

This particular inconsistency can be explained by looking at the Weimer propagated solar wind data, figure 5.11.

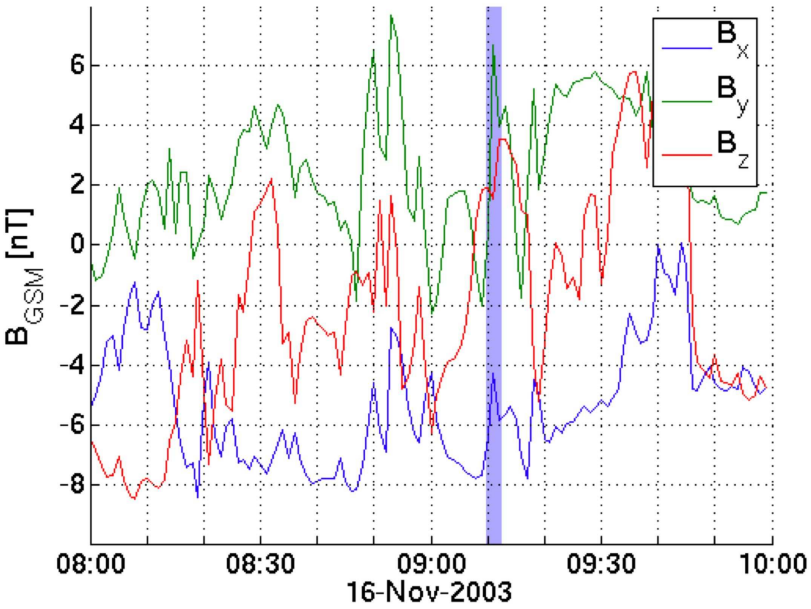

Figure 5.11: The Weimer propagated solar wind data.

Remembering that the uncertainties with this propagation technique is about 5 minutes, looking at the figure we see that there is a spike in the z-component of the magnetic field just where the crossing occurred. Just before and after the crossing, the z-component is negative. With a negative value, corresponding to a southward directed IMF, the energy flux is consistent with the theory.

In quadrant 4 we have a southward IMF and an energy output, thus it is expected that the events take place at the dayside magnetopause. The lonely point in the quadrant is event #7, this event occurred at high latitudes in the tail and are thus in need of some more discussion. Referring to table 5.1 we see that this is one event in a multi crossing series constituting of events #5-8. We see that the events preceding this event all have a dominating y-component and more importantly a northward directed IMF. This means that reconnection occurs at high latitudes and we would expect a power output if we are in the reconnection zone. Looking at panel 2 in the energy plot, figure 5.12, for this event we see clear reconnection jets and thus we are at the reconnection zone.

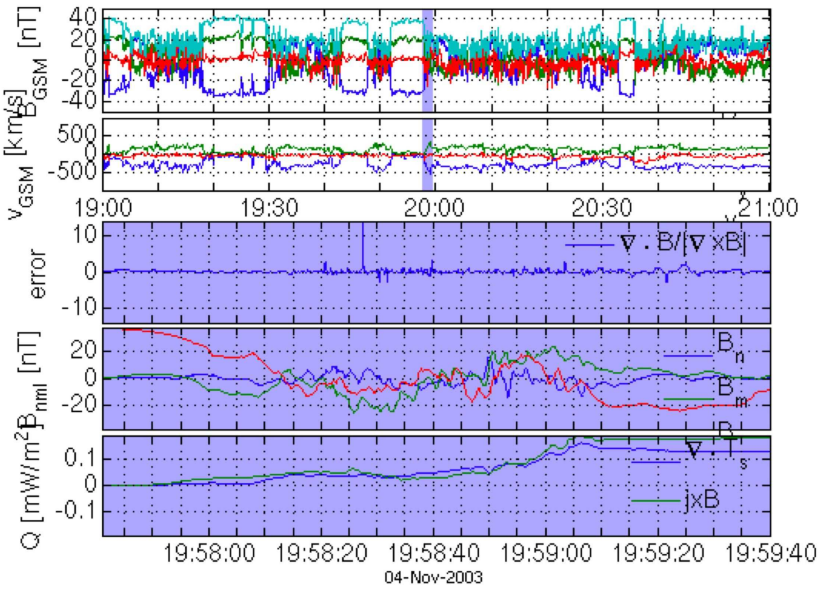

Figure 5.12: The output plot of event #7

This would then indicate that we might have a shift problem again. Looking at the Weimer propagated solar wind data in figure 5.13 we clearly see that in the uncertainty interval we mostly have a northward IMF, thus this event should probably have a northward IMF and is then consistent with the theory.

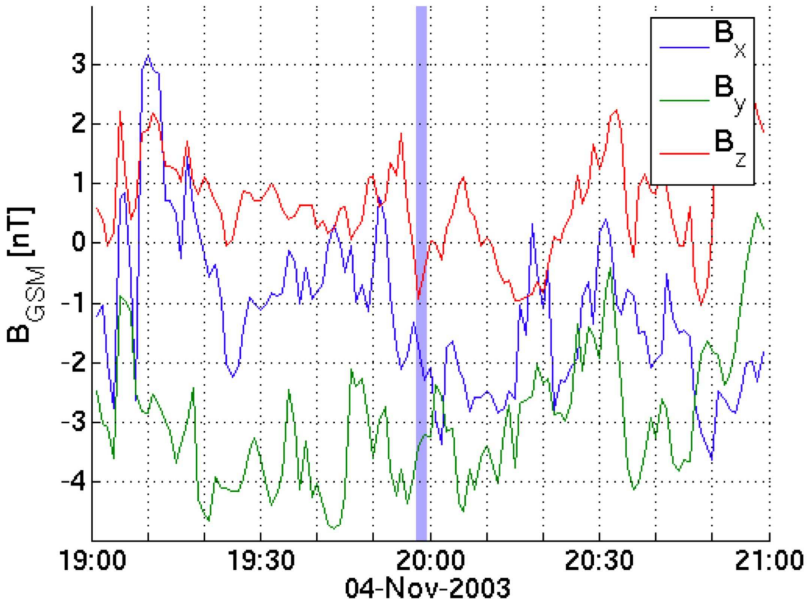

Figure 5.13: The Weimer propagated solar wind data from event #7.

Chapter 6

Conclusions

6.1 Summary

We have analyzed the transfer of energy through the magnetopause using the multi-spacecraft Cluster. For this we study Cluster magnetopause crossings. Even though there are hundreds of such magnetopause crossings, the restrictions associated with the measuring techniques used, MVA, 4-spacecraft timing and the curlometer technique, and due to other factors, i.e. magnetopause thickness and waves on the boundary, forced us to exclude a great number of them. We ended up calculating the flux for a total of 15 crossings, 8 of which were so called multiple crossings. All but one are in very good agreement with the theory developed in chapter 3, and we can with some certainty come to the following conclusions

- Load regions occur near the reconnection zones.
- On the flanks the energy transfer is strongly dependent on the location of the crossing and of the IMF orientation.

  $B_z < 0$ generator zone over a majority of the tail, with decreasing energy input closer to the neutral sheet.

  $B_z > 0$ generator regions located far away behind the reconnection zone, near zero energy flux anywhere else.

6.2 Future work

Due to the restrictions we only found 15 crossings most of which is in late 2003. In this interval there probably exists more crossings and it would be interesting and necessary to analyze these and from this maybe come to a more statistical valid conclusion. But it is inevitable that more data will be needed and this will require more time for Cluster to make more magnetopause crossings.

It's is interesting to investigate how the local energy flux change with different magnitude and direction of the IMF. That is to collect Cluster crossings from the same area and compare them. Also the opposite is important, that is how the energy transfer changes spatially when the IMF parameters are kept fairly constant. Due to the limited number of crossings used in this thesis no

such conclusions has been made, but a trend has been identified. For this to be determined much more data is needed which means more time.

Chapter 7

Acknowledgments

I would like to thank my supervisor, Lisa Rosenqvist, for always being there to answer questions and motivating me to push forwards. Also I send a big thanks to Andris Vaivads for his invaluable help during this time.

Appendix A

Program descriptions

A.1 w_cluster_func_gui.m

This program was written as an graphical user interface for calculating the energy flux for an magnetopause crossing, figure A.1 below shows the GUI.

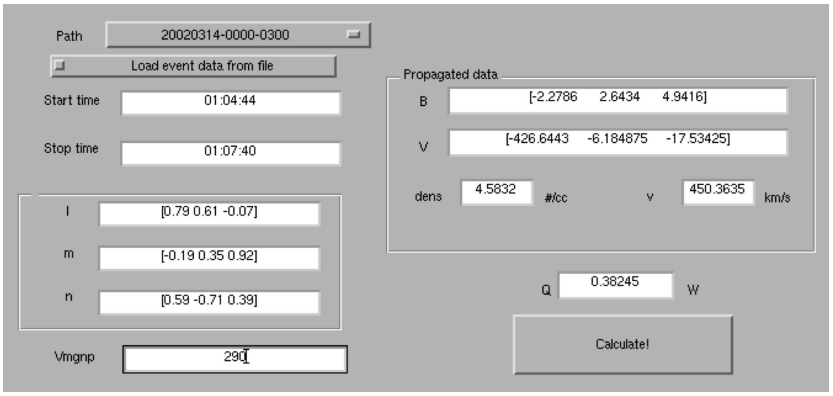

Figure A.1: The GUI developed to help with the data analysis

It demands a certain hierarchy of data according to

```
data/
----- events/
      ----- yyyymmdd-hhmm-hhmm/
            ----- mB.mat
            ----- mR.mat
            ----- mCISR.mat
      ----- yyyymmdd-hhmm-hhmm/
            ...
      ...
----- propagated/
      ----- mag/
            ----- acemagPyyyymm.mat
            ...
```

```
----- plasma
      ----- aceplasmaPyyyymm.mat
      ...
```

under the `events` catalogue all the crossing are stored in folders. The format is necessary since the GUI reads all the folder names in this catalogue and fills the listbox at the top left with data based on these. Under the catalogue `propagated` the propagated solar wind data recedes, both for the plasma and magnetic data. This data is automatically fetched and the textareas on the right of the GUI is filled. In the textfields named Start and Stop time the start and stop times of the crossings must be entered on the format `hh:mm:ss`. After this the user must enter the three *nml*-vectors of the magnetopause and finally the velocity of the magnetopause at the bottom textfield. This data is then saved to a file, this file can be loaded by checking the `Load event data from file`. The calculations are performed when the `Calculate!` button is clicked, the result is shown in the textarea just above the button.

A.2 shue_magpause_locate.m

This program was written to provide the means to compare the measured normals from MVA and timing with a theoretical normal. The program is using the Shue et al. magnetopause model

$$r = r_0 \left(\frac{2}{1 + \cos\theta} \right)^{\alpha},$$

where r is radial distance and θ is solar zenith angle. The two parameters r_0 and α represents the standoff distance and the level of tail flaring respectively defined as

$$r_0 = 10.22 + 1.29 \tanh 0.184(B_z + 8.14)) D_p^{\frac{-1}{6.6}}$$

$$\alpha = (0.58 - 0.007 B_z)(1 + 0.024 \log D_p)$$

where B_z is the z_{gsm} component of the IMF and D_p the solar wind dynamic pressure defined as

$$D_p = 1.95e - 6 * n v_{sw}^2,$$

here v_{sw} is the solar wind velocity and n is the solar wind density. The output of the program is presented in figure A.2. In the figure we see the location of one of the Cluster satellites, C1, marked by a 1. The closest point on the magnetopause is marked by a red square and the calculated normal is marked with a blue line. Also the program outputs the normal to the matlab terminal.

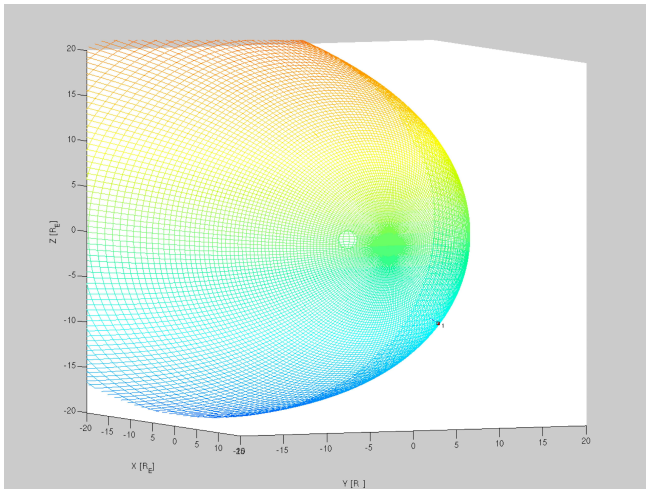

Figure A.2: The output from the magnetopause location program.

Bibliography

[1] S Akasofu. Energy coupling between the solar wind and the magnetosphere. *Planet Space Science*, 27:425–431, 1979.

[2] Professor Andre Balogh. Cluster ready for lift-off. `http://www.pparc.ac.uk/frontiers/archive/feature.asp?id=7F3&style=feature`. Read 2006-10-19.

[3] ESA. Csdsweb plots. `http://www.cluster.rl.ac.uk/csdsweb-cgi/csdsweb_pick`.

[4] Lisa Rosenqvist et. al. Magnetospheric energy budget during huge geomagnetic activity using cluster and groundbased data. *Journal of Geophysical Research*, 111, 2006.

[5] Luhmann et al. Patterns of potential megnetic field merging sites on the dayside magnetopause. *Journal of Geophysical Research*, 89(A3):1739–1742, 1984.

[6] Shue J. H. et al. A new functional form to study the solar wind control of the magnetopause size and shape. *Journal of Geophysical Research*, 102:9497–9511, 1997.

[7] Weimer D. R. et al. Predicting interplanetary magnetic field (imf) propagation delay time using minimum variance technique. *Journal of Geophysical Research*, 108, 2004.

[8] et.al. Margaret G. Kivelson, Christopher T. Russel. *Introduction to Space Physics*. Cambridge University Press, 1997.

[9] Los Alamos National Security. Ace pictures. `http://swepam.lanl.gov/acepics/ace4.JPG`. Read 2006-10-19.